

## Supplemental Information

### Higher-order SPOP assembly reveals a structural basis for cancer mutant dysfunction

Matthew J. Cuneo<sup>1#</sup>, Brian G. O'Flynn<sup>1#</sup>, Yu-Hua Lo<sup>1,2</sup>, Nafiseh Sabri<sup>1</sup>, Tanja Mittag<sup>1,3\*</sup>

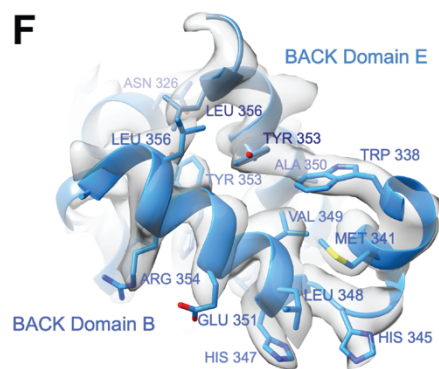
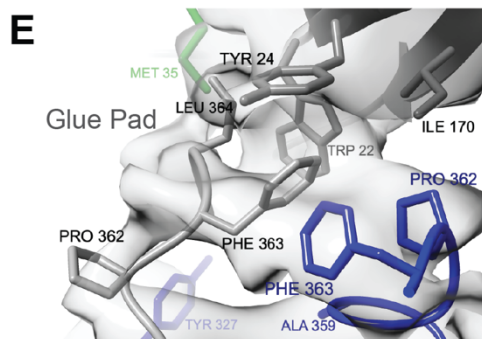
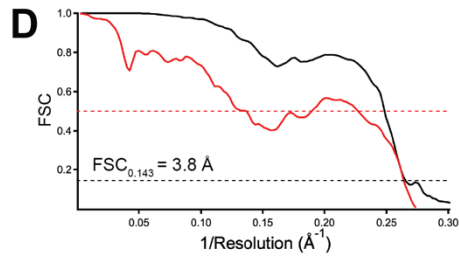
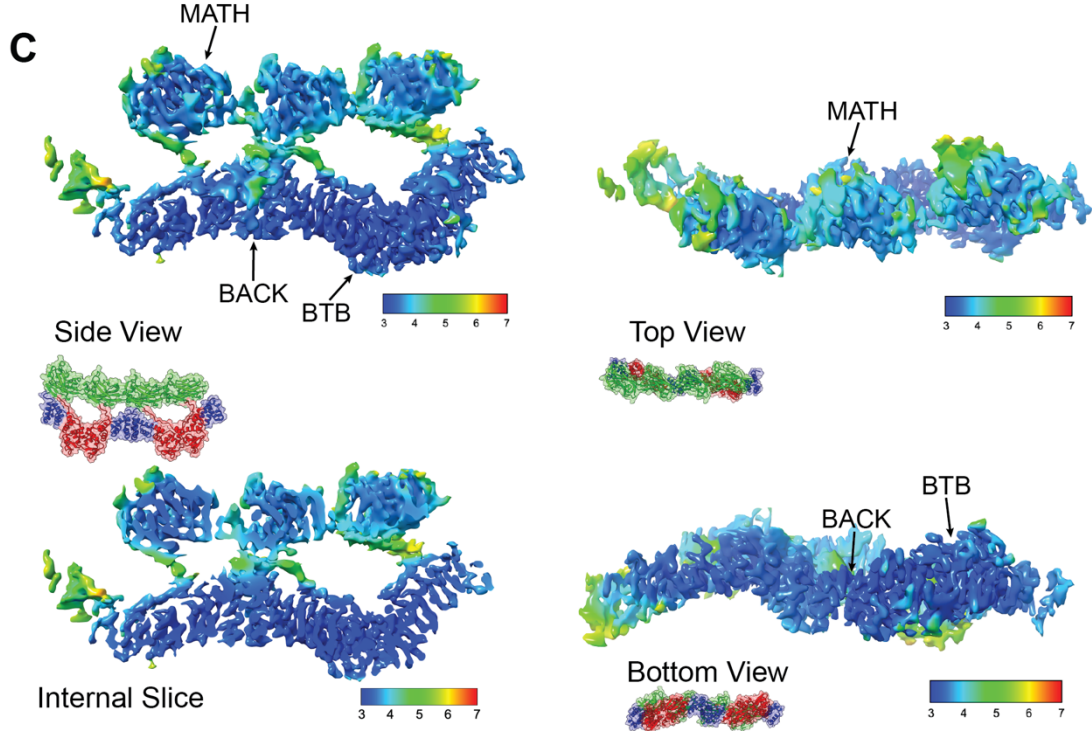
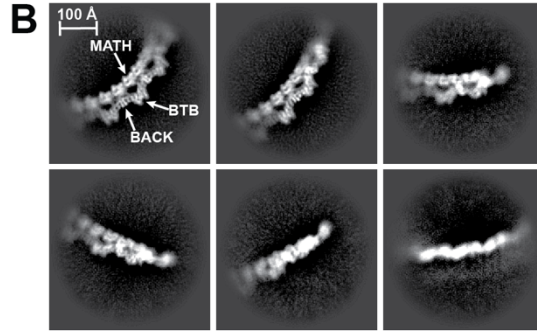
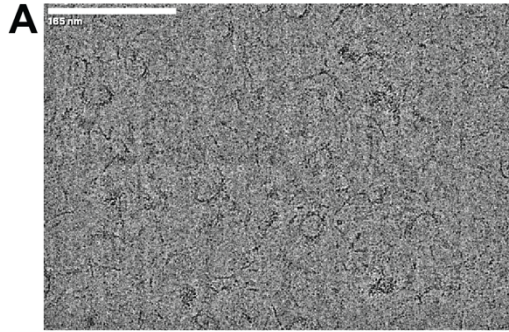
<sup>1</sup> Department of Structural Biology, St. Jude Children's Research Hospital, Memphis, TN 38103, USA

<sup>2</sup> Current address: Eli Lilly & Company, San Diego, CA 92121, USA

<sup>3</sup> Lead contact

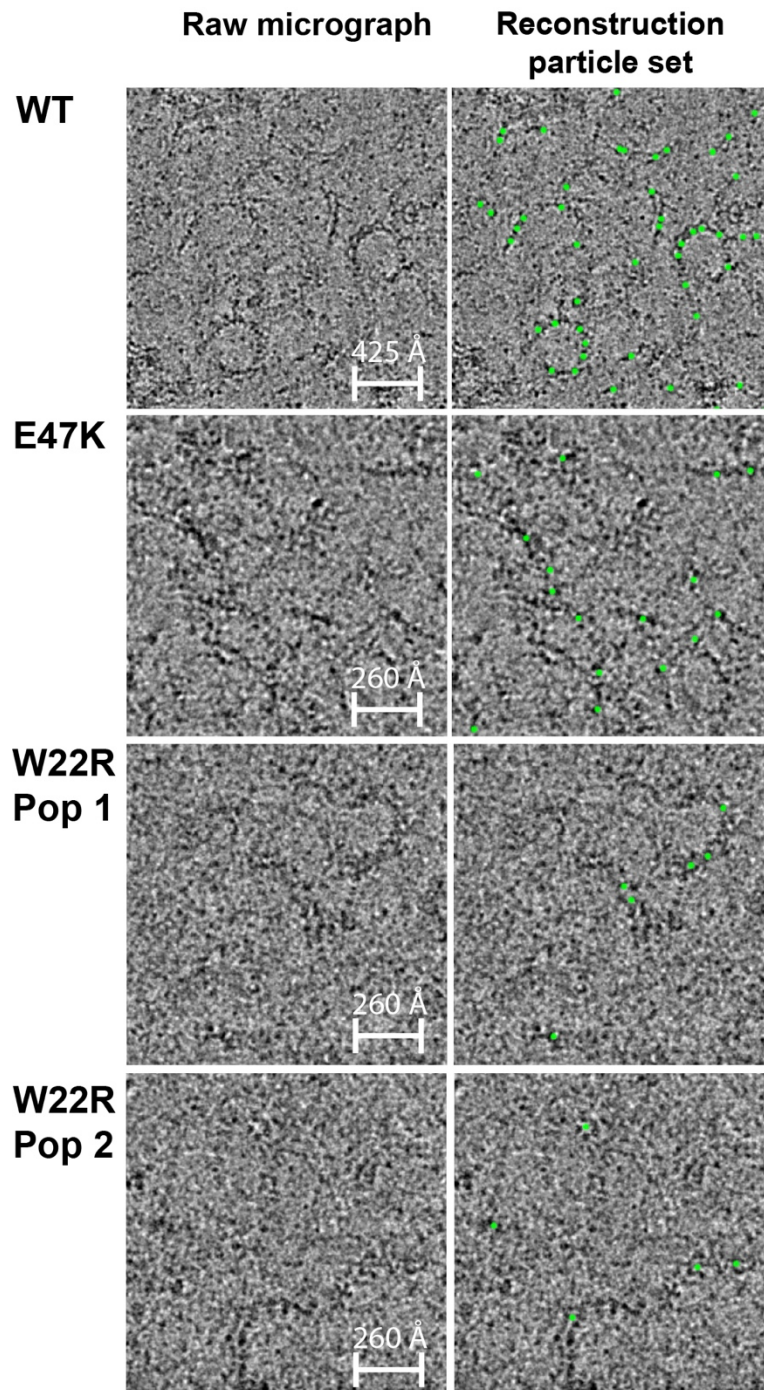
# These authors contributed equally.

\* Correspondence: [anja.mittag@stjude.org](mailto:anja.mittag@stjude.org)

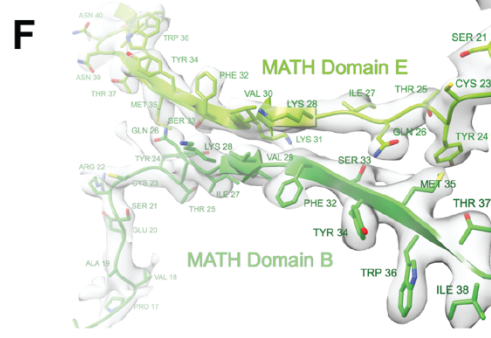
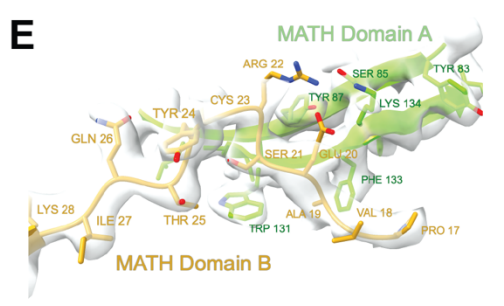
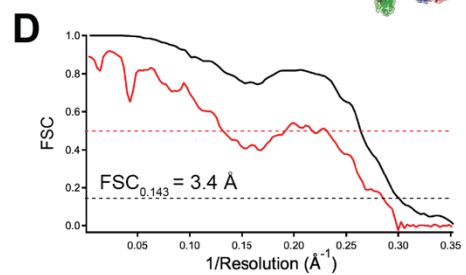
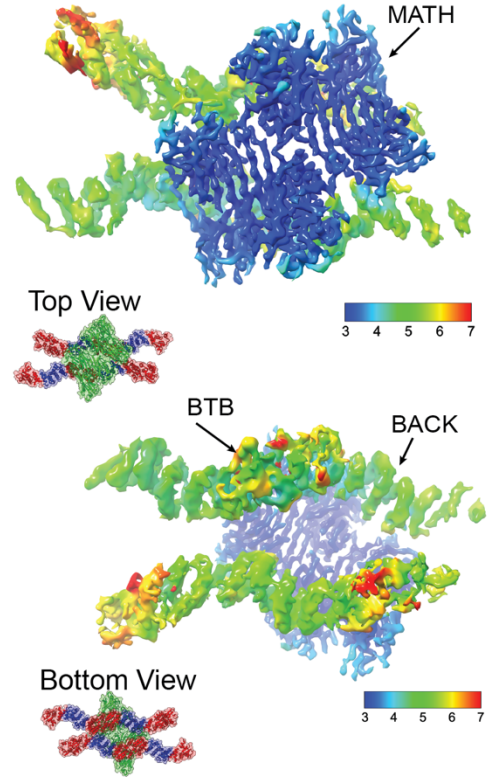
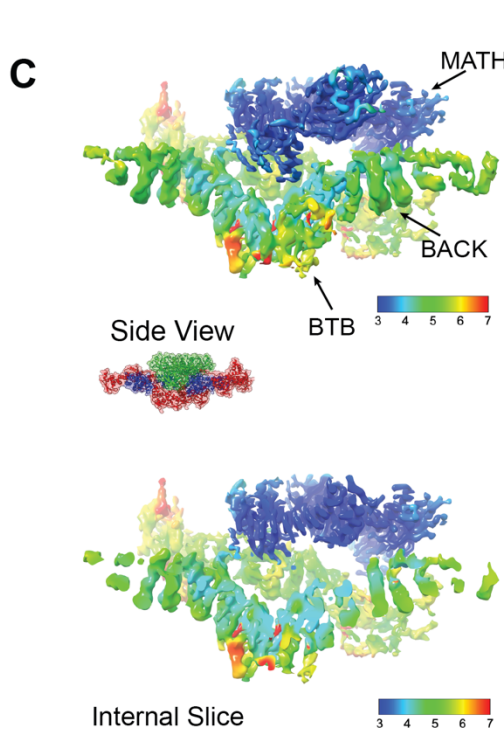
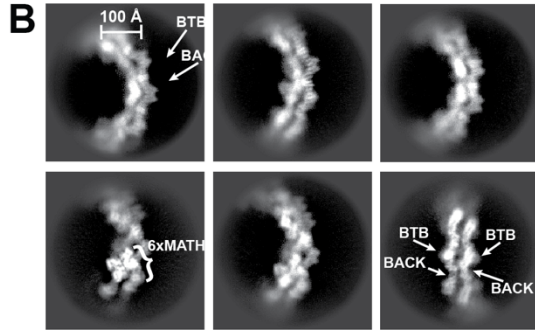
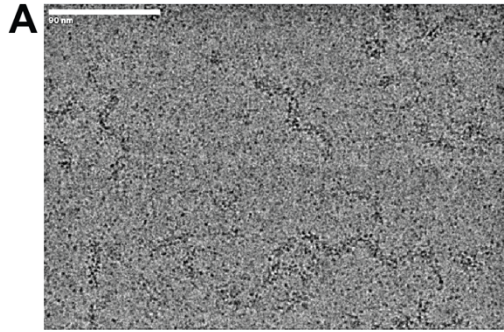


**Supplementary Figure 1, Related to Figure 2. Cryo-EM data and validation of WT SPOP structure.**

(A) Representative cryo-EM micrograph. Filaments had various lengths from very short to long. We previously characterized self-association of a shorter SPOP<sup>28-359</sup> construct into oligomers in solution and showed that association was isodesmic (i.e., each addition of a new unit was governed by the same affinity) and resulted in the expected exponential size distribution, i.e., large numbers of small oligomers coexisted with decreasing numbers of larger oligomers (Marzahn et al. EMBO J 2016). We hypothesize that self-association of full-length SPOP is also isodesmic in nature, and the size distribution is therefore also exponential. Freezing results in the perturbation of some filaments at the air-water interface, which may lead to changes in the apparent size distribution, which was thus not quantified. (B) 2D class averages of WT SPOP. (C) Side view, top view, and bottom view of sharpened cryo-EM map colored according to calculated local resolution. Side view is also shown with vertical slice to show interior resolution. Inset images show orientation and are colored by domain type (MATH, green; BTB, red; BACK, blue). (D) Fourier Shell Correlation (FSC) curves calculated after masking (black) with the gold standard criteria (FSC threshold = 0.143) estimating a resolution of 3.8 Å. Map-to-model FSC curve (red) calculated between the refined structure and the full map (FSC threshold = 0.5). (E) Sharpened map and model view of glue pad region. (F) Sharpened map and model showing details of the BACK-BACK interface.

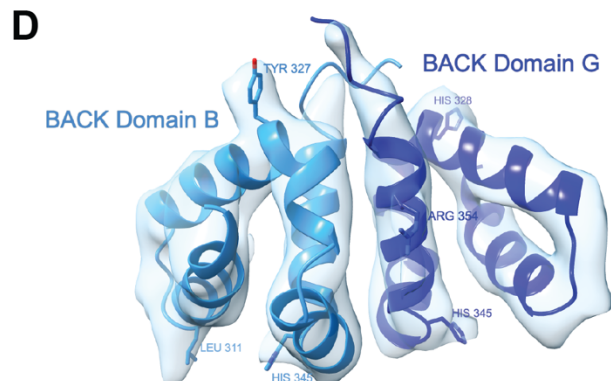
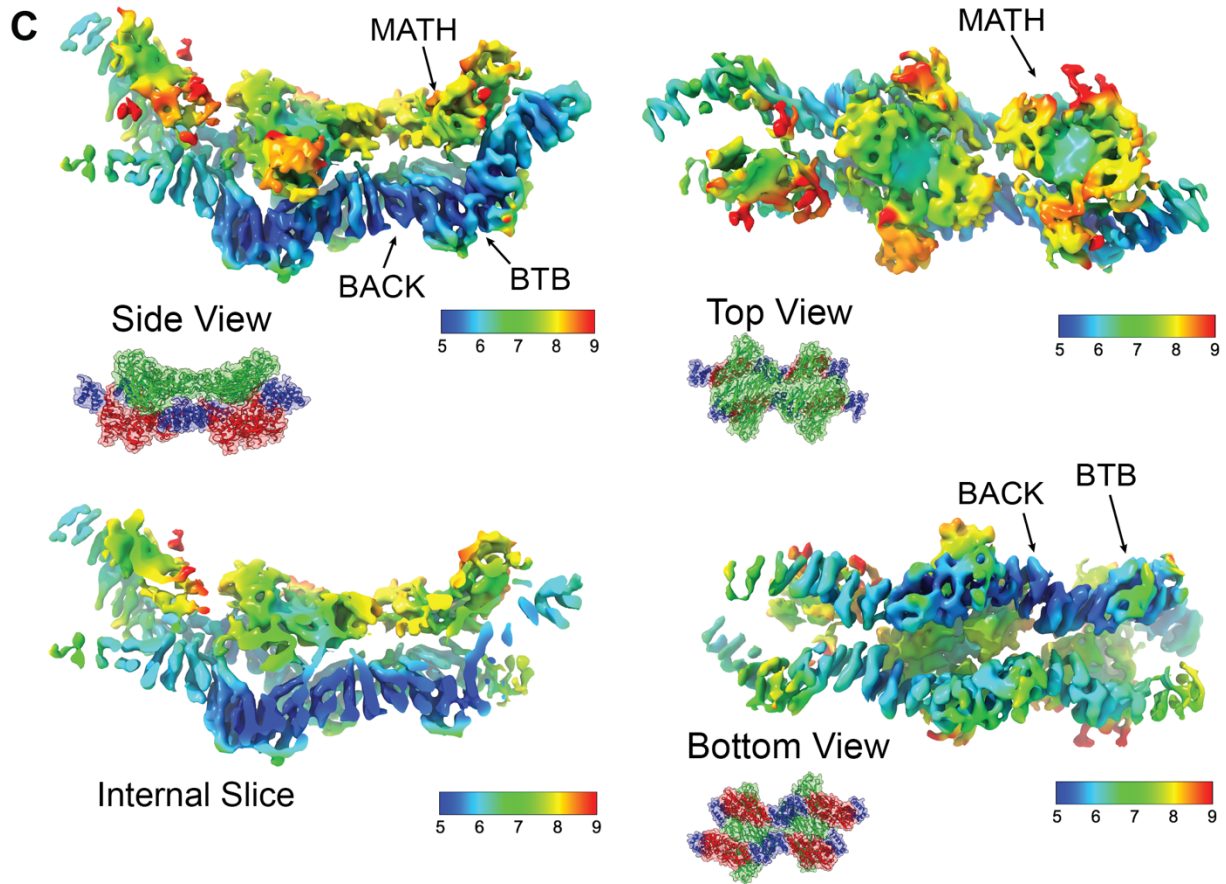
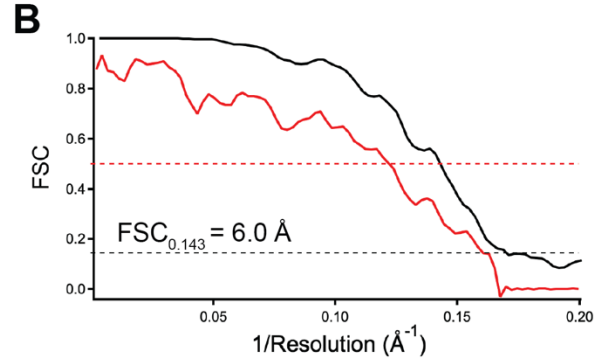
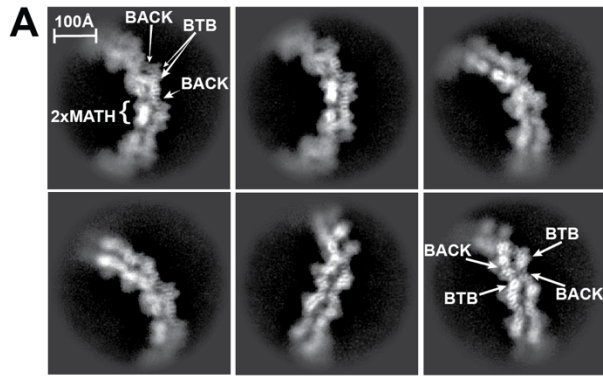


**Supplementary Figure 2, related to STAR Methods. Short segments along the filaments were extracted as individual particles. (Left)** Small sections of raw micrographs showing filaments. **(Right)** Center of the position of each particle used for reconstruction.



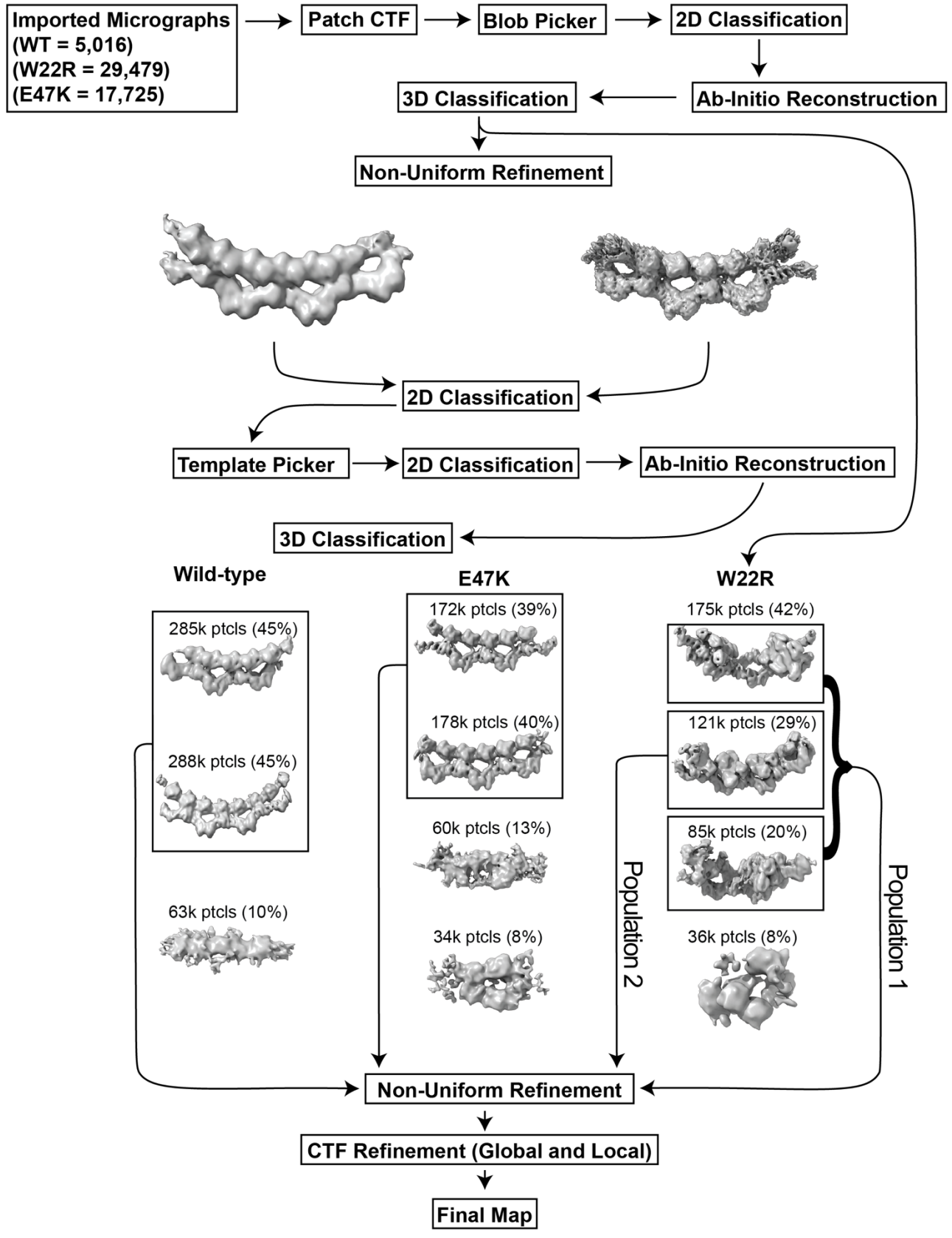
**Supplementary Figure 3, Related to Figure 4. Cryo-EM data and structure validation of SPOP W22R population 1.**

(A) Representative cryo-EM micrograph. (B) 2D class averages of W22R SPOP population 1. (C) Side view, top view, and bottom view of cryo-EM map colored according to calculated local resolution. Side view is shown with vertical slice to show interior resolution. Inset images show orientation and are colored by domain type (MATH, green; BTB, red; BACK, blue). (D) Fourier Shell Correlation (FSC) curves calculated after masking (black) with the gold standard criteria (FSC threshold = 0.143) estimating a resolution of 3.4 Å. Map-to-model FSC curve (red) calculated between the refined structure and the full map (FSC threshold = 0.5). (E) Sharpened map and model showing inter-monomer interactions between MATH domain (chain A) and the pseudo-SB motif in the N-terminus (of chain B, gold). (F) Sharpened map and model showing assembly of side-by-side MATH domains (B and E) with inter-monomer  $\beta$ -sheet extension.



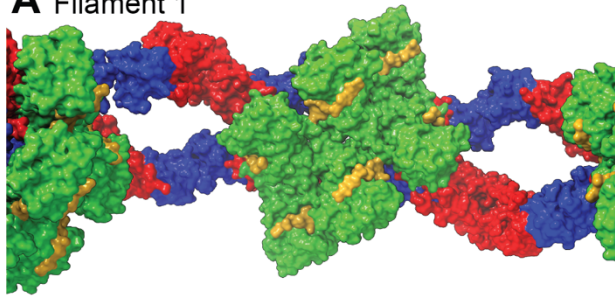
**Supplementary Figure 4, Related to Figure 4. Cryo-EM 2D classes and structure validation of SPOP W22R population 2.**

(A) 2D class averages of W22R population 2. (B) Fourier Shell Correlation (FSC) curves calculated after masking (black) with the gold standard criteria (FSC threshold = 0.143) estimating a resolution of 6.0 Å. Map-to-model FSC curve (red) calculated between the refined structure and the full map (FSC threshold = 0.5). (C) Side view, top view, and bottom view of cryo-EM map colored according to calculated local resolution. Side view is shown with vertical slice to show interior resolution. Inset images show orientation and are colored by domain type (MATH, green; BTB, red; BACK, blue). (D) Sharpened map and model of BACK domain dimer.

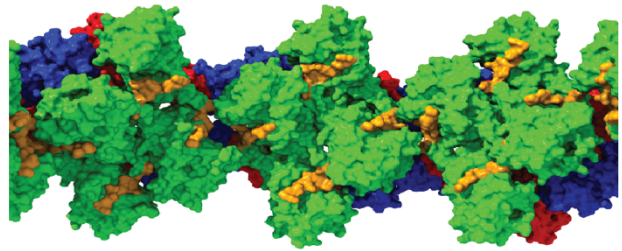


**Supplementary Figure 5, related to STAR Methods. Flowchart of cryo-EM data processing steps.** A general strategy used for map reconstruction for SPOP WT and mutants. An initial step of blob picking using a subset of micrographs generated a set of 2D classes. These were used for template picking across the entire dataset. Blob picking using the entire dataset was sufficient for W22R, and thus, template picking was skipped. 3D maps were then generated, and junk particles filtered out. CTF refinement and non-uniform refinement followed, generating the final high-resolution maps. See also Methods.

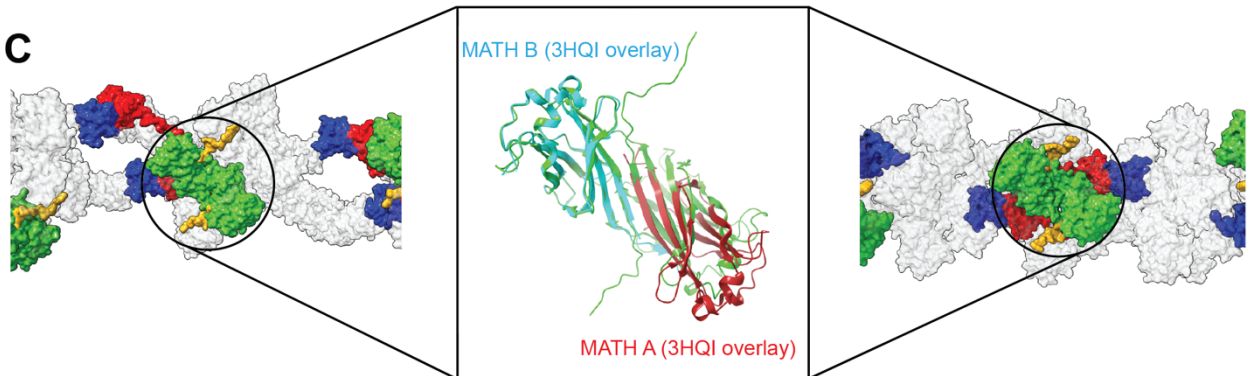
**A** Filament 1



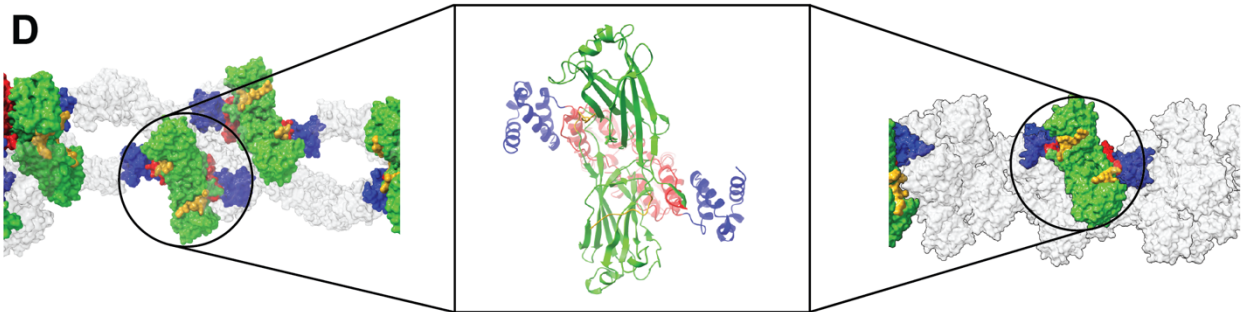
**B** Filament 2



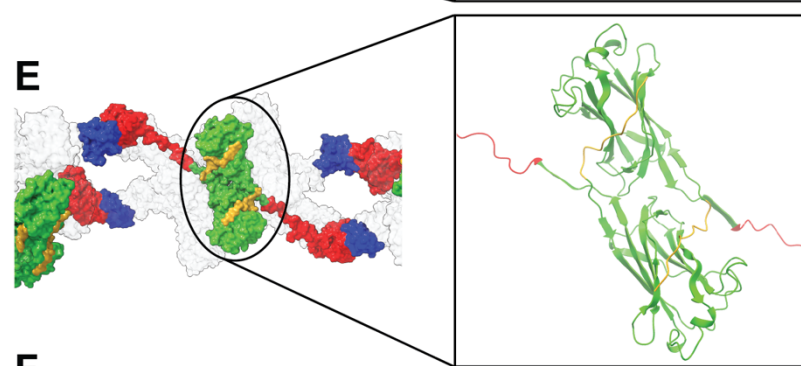
**C**



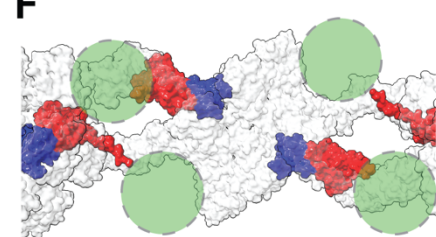
**D**



**E**

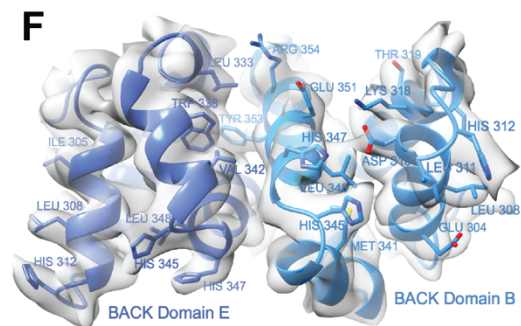
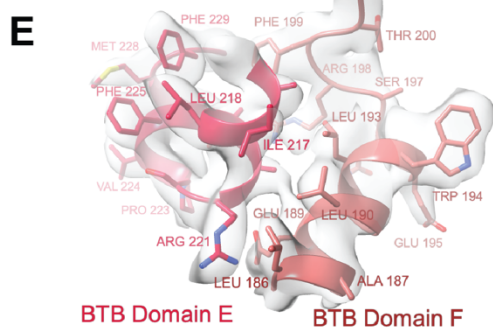
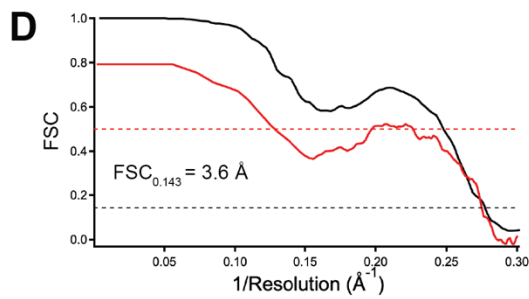
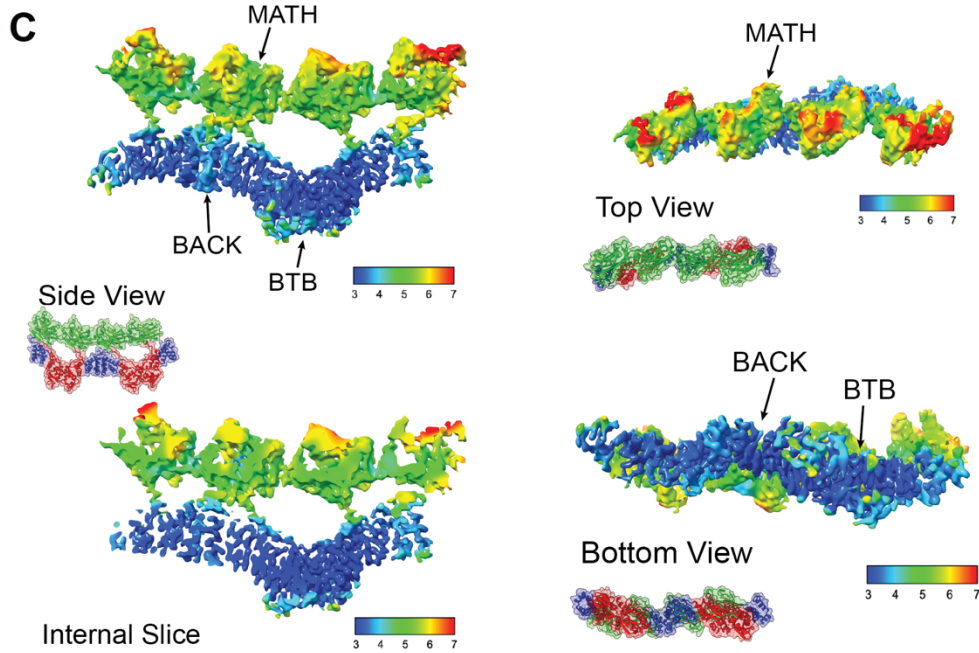
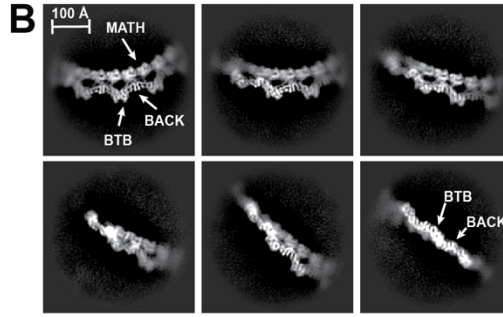
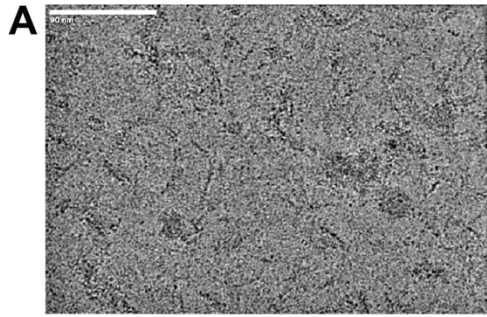


**F**



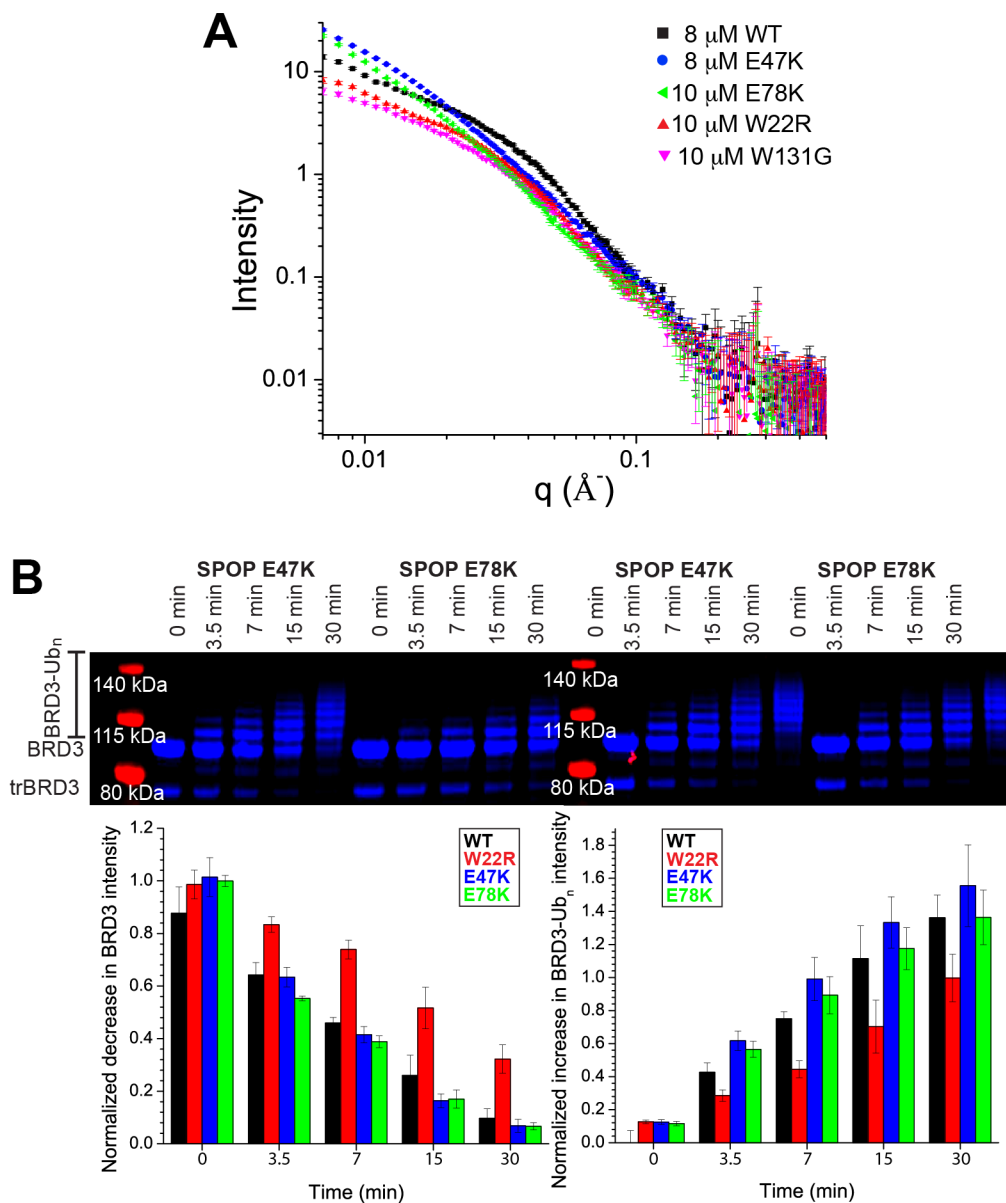
**Supplementary Figure 6, Related to Figure 4. Assembly schematic of populations 1 and 2 of SPOP W22R.**

(A) W22R model from population 1 and (B) from population 2 showing MATH domains (green), BTB domains (red), BACK domains (blue), and interconnecting pseudo-SB motifs (residues 17-25 including R22, gold). (C) Interaction between two MATH monomers which form extensive contacts between their respective  $\beta$ 2 strands in a head-to-head orientation. This interaction is seen in both populations and has been observed previously in a crystal structure of the SPOP<sup>28-337</sup> dimer (PDB: 3HQI<sup>1</sup>), which is superimposed (center panel, red and cyan) onto the W22R model (green). (D) Detailed representation of interactions made through pseudo-SB motifs seen in both populations, and (E) one interaction seen only in population 1. (F) Extra flanking MATH domains expected to be located within the green circles in population 1. This is implied by stoichiometry of BTB and BACK domains (shown in red and blue respectively) and the appearance of corresponding density at lower map thresholds. These MATH domains are not locked in place by any interdomain interactions and do not have high enough resolution density to be modeled.



**Supplementary Figure 7, Related to Figure 5. Cryo-EM data and validation of SPOP E47K structure.**

(A) Representative cryo-EM micrograph. (B) 2D class averages of E47K SPOP. (C) Side view, top view, and bottom view of cryo-EM map colored according to calculated local resolution. Side view is shown with vertical slice to show interior resolution. Inset images show orientation and are colored by domain type (MATH, green; BTB, red; BACK, blue). (D) Fourier Shell Correlation (FSC) curves calculated after masking (black) with the gold standard criteria (FSC threshold = 0.143) estimating a resolution of 3.6 Å. Map-to-model FSC curve (red) calculated between the refined structure and the full map (FSC threshold = 0.5). (E) Map and model showing details of interaction between BTB domains. (F) Map and model showing details of interaction between BACK domains.



**Supplementary Figure 8, Related to Figure 6.** (A) Raw SAXS scattering curves of WT SPOP and mutants used in this study. The error bars represent the S.D. from reduction from 2D to 1D data. (B) *In vitro* ubiquitination assays with 0.5:1 CRL (complex:SPOP). E47K and E78K SPOP marginally increase ubiquitination activity *in vitro*, W22R does not. *In vitro* ubiquitination assays with CRL3<sup>SPOP</sup> were performed as described previously (Zhuang et al, 2009) using fluorescently labeled BRD3 as a substrate, WT SPOP, and the characterized endometrial cancer mutants W22R, E47K and E78K SPOP. Top, ubiquitination efficiency was monitored by SDS-PAGE and fluorescent imaging in 3 independent assays. Bottom left and right, quantification of the decrease of unmodified BRD3 and of the increase of ubiquitinated BRD3 (Ub<sub>n</sub>-BRD3) as a function of time. The mean value  $\pm$  the S.D. are reported.

## Supplemental References

- S1. Zhuang, M., Calabrese, M.F., Liu, J., Waddell, M.B., Nourse, A., Hammel, M., Miller, D.J., Walden, H., Duda, D.M., Seyedin, S.N., et al. (2009). Structures of SPOP-substrate complexes: insights into molecular architectures of BTB-Cul3 ubiquitin ligases. *Mol Cell* 36, 39-50. [10.1016/j.molcel.2009.09.022](https://doi.org/10.1016/j.molcel.2009.09.022).